IEEE Access
Multidisciplinary | Rapid Review | Open Access Journal

Received 9 November 2022, accepted 28 November 2022, date of publication 1 December 2022,
date of current version 7 December 2022.

Digital Object Identifier 10.1109/ACCESS.2022.3225876

RESEARCH ARTICLE

Hybrid Double-RIS and DF-Relay for Outdoor-to-Indoor Communication

GUANG-HUI LI[1], DIAN-WU YUE[1,2], (Senior Member, IEEE), SI-NIAN JIN[1], (Member, IEEE), AND QING HU[1], (Member, IEEE)

[1]College of Information Science and Technology, Dalian Maritime University, Dalian, Liaoning 116026, China
[2]State Key Laboratory of Millimeter Waves, Southeast University, Nanjing, Jiangsu 210096, China

Corresponding author: Dian-Wu Yue (dwyue@dlmu.edu.cn)

ABSTRACT Reconfigurable intelligent surface (RIS) is a promising solution to enhance the energy and spectral efficiency of future wireless networks. The system with single RIS might not be able to provide sufficient line-of-sight (LoS) links for outdoor-indoor communication, which often limits the signal transmission distance and coverage range. This paper first proposes a novel hybrid double-RIS and full-duplex (FD) decode-and-forward (DF) relay aided system to eliminate the impact of building occlusion and penetration loss in outdoor-indoor communication. Expressions of the upper bound for the ergodic spectral efficiency (ESE) are derived and match the simulation results well. To maximize the ESE, two algorithms are proposed for passive beamforming of the RIS: optimal phase shifts (OPS) and generalized cross-entropy (GCE) algorithm. Results show that the OPS can provide a power gain of the square of the RIS elements' number. The proposed GCE-based discrete phase shifts algorithm can achieve a good performance on the energy efficiency. An optimal power allocation (OPA) scheme between the source and relay is also proposed to maximize the spectral efficiency. Numerical results demonstrate the performance advantage of the OPA over the equal power allocation (EPA).

INDEX TERMS Reconfigurable intelligent surface, decode-and-forward relay, ergodic spectral efficiency, passive beamforming, outdoor-to-indoor communication.

I. INTRODUCTION

With the rapid development of the Internet of Things (IoT) and the wireless communication, mobile data traffic has witnessed an unprecedented growth. By smartly reconfiguring the wireless propagation environment to enhance the communication performance with low cost, reconfigurable intelligent surface (RIS) has been proposed as one of the key technologies for the sixth-generation (6G) wireless networks. The use of RIS could establish a foundation for new wireless networks to realize the Internet-of-Everything (IoE) era. In general, a RIS is composed of a large number of low-cost passive elements [1], [2]. Each element can reflect the incident signal by inducing an amplitude and/or phase change to achieve the fine-grained three-dimensional (3D) passive beamforming. By properly adjusting the passive beamforming, the signal reflected by the RIS can add constructively to enhance the power of the desired signal at the receiver, or destructively cancel the undesired signal to avoid interference and enhance security/privacy [3].

Research on the RIS has received significant attention in both academia and industry. For example, many works focusing on the performance of RIS-aided systems has been published in [3], [4], [5], [6], [7], [8], and [9]. In particular, for a single-RIS-assisted system, the authors in [3] and [4] investigated the optimization of continuous and discrete passive beamforming, respectively. For the multi-RIS-assisted systems, the authors in [6], [7], and [8] investigated a system in which two RISs are deployed in parallel to assist data transmission. In [9], the authors investigated a cooperative double-RIS-aided wireless communication system, in which two RISs cooperated in serial to eliminate channel blockage. To address the severe signal blockage and achieve larger coverage, the authors proposed a new multi-hop models

The associate editor coordinating the review of this manuscript and approving it for publication was Olutayo O. Oyerinde.

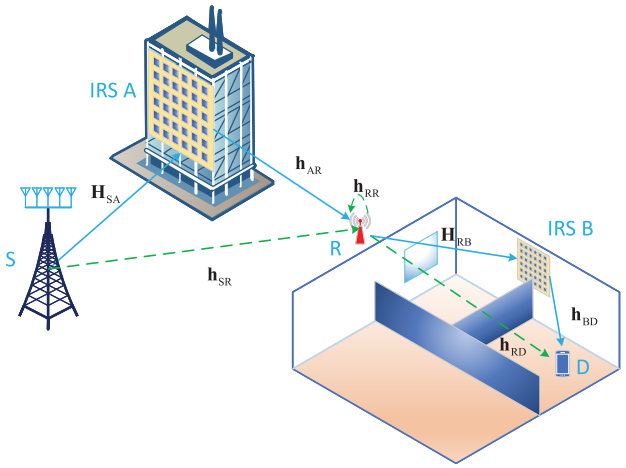

FIGURE 1. The proposed hybrid double-RIS and FD DF-relay aided system.

by introducing multiple passive and controllable RISs [10]. Benefited from its features, the RIS can be fabricated in very compact size with light weight and installed in building facades, ceilings, walls, laptops, clothes, etc. However, the methodology developed for multi-hop RIS-assisted systems is still a challenge due to different reflecting mechanisms and channel models with the active relays. Moreover, the large-scale fading attenuation of a multi-hop RIS-assisted systems is proportional to the product of the multi-hop distances [11], [12]. Hence, the path loss is likely to increase with the number of hops. The amplitude loss caused by RIS reflection is also a problem to be addressed. The current researches often assume no amplitude loss, but the impact of imperfect reflection in multi-hop RIS assisted systems will be very serious which cannot be neglected. Therefore, arranging multiple cascaded RISs may make the overall reflection loss and path loss too large to enable reliable communication. The authors recently compared a RIS-aided system with the amplify-and-forward (AF) /decode-and-forward (DF) relays systems and found that it requires hundreds of elements for the RIS-aided system to outperform the relay systems [13], [14]. However, conventional relays are lacking the ability of focusing the signal, which limits the ability for wireless coverage and increases the interference to unintended receivers. Further, the MIMO relays are costly and bulky with high power consumption.

To address the high power consumption of multi-hop relays and high performance loss of multi-hop RISs systems, combining relay and RIS seems like a more practical solution. Following this direction, the authors proposed a novel relay-aided RIS architecture which illustrates that relay-aided RIS with a DF relay achieves higher gain compared to the relay-aided RIS with a AF relay [15]. In principle, RIS is quite similar to the AF relay. The main difference is that RIS does not use any active transmit module (e.g., radio-frequency chains, power amplifier) but only reflects the received signal as a passive array. The results also demonstrated that the RIS with hundreds of reflecting elements can replace a multi-antenna AF relay [3]. Then the authors proposed a hybrid RIS and half-duplex (HD)-DF relay network and a RIS-assisted full-duplex (FD) relay network successively [16], [17]. The authors in [18] introduced two hybrid transmission schemes that combine a passive RIS with a DF relay in a synergistic manner: (i) joint RIS and relay transmission scheme, and (ii) integrated RIS and relay transmission scheme. Many works have verified that the closer the RIS is to the transmitter or receiver, the better the system performance is. In addition, the RISs in all of the above systems need to be deployed jointly with the relay, which is detrimental for flexible deployment of the RISs while enabling reliable performance. Thus, more efficient and reliable system models jointly aided by relay and RISs are required.

To effectively assist an outdoor source to communicate with an indoor destination, we propose a novel hybrid double-RIS and FD DF-relay aided system as illustrated in Fig. 1, the RISs are near the source and the destination respectively. The reasons to adopt the double-RIS and FD DF-relay are as follows. First, compared with the muti-hop relays or muti-hop RISs systems, hybrid the DF relay and RISs architecture can reduce the cost while reducing the reflection loss. Second, an FD relay equipped with omnidirectional antennas can assist the RIS to reflect and avoid blind areas. Third, due to the characteristics of DF relay, improving the performance of a single hop with single RIS may be ineffective.

The main technical contributions of this paper are summarized as follows:

- We propose a novel hybrid double-RIS and FD DF-relay aided system to assist in the communication between an outdoor source and an indoor destination.
- To obtain the power scaling law, we derive the upper bounds of the ergodic spectral efficiency (ESE) in different channel environments, which demonstrate the effect of the RISs and the relay intuitively.
- To improve the energy and spectral efficiency, two optimization methods for passive beamforming are proposed for the RISs: optimal phase shifts (OPS) and generalized cross-entropy (GCE) algorithms, which perform good on ESE and EEE, respectively. Moreover, the optimal power allocation (OPA) scheme between the source and relay is performed to further enhance the performance of the network.
- Our results demonstrate that the proposed hybrid double-RIS and FD relay system significantly outperforms the system using HD relay or only RISs.

The remainder of this paper is organized as follows. Section II describes the system and channel models. We analyze the performance difference of HD and FD relays in Section III. Section IV addresses optimization of passive beamforming and power allocation. Section V provides simulation results to demonstrate the effectiveness of the proposed system and method of optimization. Finally, conclusions are given in Section VI.

Notations: Scalars are denoted by italic letters. Boldface upper and lower case symbols represent matrices and vectors, respectively. Hermitian transpose and matrix inversion operators are represented by $(\cdot)^H$ and $(\cdot)^{-1}$, respectively. $\mathbb{C}^{A\times B}$ denotes the space of $A \times B$ complex-valued matrices. We use $\mathcal{CN}\left(\mu, \sigma^2\right)$ to denote a circularly symmetric complex Gaussian distribution (CSCG) with mean μ and variance σ^2, and $\sim$ stands for "distributed as". $\{\cdot\}$ represents a collection of elements. $\|\cdot\|$ represents the Euclidean norm. $|\cdot|$ denotes the absolute value of a complex number.

II. SYSTEM AND CHANNEL MODELS

A. SYSTEM MODEL

As illustrated in Fig. 1, we consider a communication system which comprises a source (S), a FD DF relay (R), a destination (D), and two RISs (A and B). We assume a multi-antenna S with N_{S} antennas and a single-antenna D, which are far apart from each other and there is no direct link between them [6], [10]. RIS A and RIS B are deployed to assist communication, which have N_{A} elements and N_{B} elements, respectively. Furthermore, we adopt a DF relay in which the transmitter and receiver have N_{R} and single antennas respectively. We define $\mathbf{H}_{\mathrm{SA}} \in \mathbb{C}^{N_{\mathrm{A}}\times N_{\mathrm{S}}}$, $\mathbf{h}_{\mathrm{AR}} \in \mathbb{C}^{1\times N_{\mathrm{A}}}$, $\mathbf{H}_{\mathrm{RB}} \in \mathbb{C}^{N_{\mathrm{B}}\times N_{\mathrm{R}}}$, $\mathbf{h}_{\mathrm{BD}} \in \mathbb{C}^{1\times N_{\mathrm{B}}}$, $\mathbf{h}_{\mathrm{SR}} \in \mathbb{C}^{1\times N_{\mathrm{S}}}$, and $\mathbf{h}_{\mathrm{RD}} \in \mathbb{C}^{1\times N_{\mathrm{R}}}$ as the channel matrices (or vectors) between S $\rightarrow$ A, A $\rightarrow$ R, R $\rightarrow$ B, B $\rightarrow$ D, S $\rightarrow$ R, and R $\rightarrow$ D, respectively. At time instant t, S transmits the signal $x_{\mathrm{S}}(t)$ to R, and R transmits the signal $x_{\mathrm{R}}(t)$ to D. $\mathbf{h}_{\mathrm{RR}}$ is the channel between the transmitter and receiver of the relay, which represents the loop interference. Due to the large path loss and penetration loss, the power of signals transmitted from A to D and that are reflected by the RIS more than once is very small and can be ignored [3], [16].

Assuming the reflection coefficient of the RISs at A and B is ρ [3], we define the diagonal matrices $\mathbf{\Theta}_q = \mathrm{diag}\left(\rho e^{j\varphi(q,1)}, \ldots, \rho e^{j\varphi(q,N_q)}\right), q \in \{\mathrm{A}, \mathrm{B}\}$ as the interaction matrices of the RISs, where $\varphi(q, n) \in [0, 2\pi)$ is the phase shift of the nth reflecting element.

In the first hop, S transmits $x_{\mathrm{S}}(t)$ to both A and R, and A reflects the incident signal towards R. Therefore, the received signal at R can be represented as

$$y_{\mathrm{R}}(t) = \sqrt{P_1} f_{\mathrm{S}} \left(\mathbf{h}_{\mathrm{AR}}\mathbf{\Theta}_{\mathrm{A}}\mathbf{H}_{\mathrm{SA}} + \mathbf{h}_{\mathrm{SR}}\right) x_{\mathrm{S}}(t) + n_{\mathrm{RI}} + n_{\mathrm{R}}, \quad (1)$$

where P_1 is the transmitted powers in the first hop, respectively, $n_{\mathrm{R}} \sim \mathcal{CN}\left(0, \sigma_{\mathrm{n}}^2\right)$ is the additive white Gaussian noise (AWGN) component at R, f_{S} is the $N_{\mathrm{S}} \times 1$ precoder used by S that satisfies $\|f_{\mathrm{C}}\|^2 = 1$, n_{RI} is the self-interference of R.

With the maximum ratio transmission (MRT), the precoder at S is given by

$$f_{\mathrm{S}} = \frac{\left(\mathbf{h}_{\mathrm{AR}}\mathbf{\Theta}_{\mathrm{A}}\mathbf{H}_{\mathrm{SA}} + \mathbf{h}_{\mathrm{SR}}\right)^H}{\left\|\mathbf{h}_{\mathrm{AR}}\mathbf{\Theta}_{\mathrm{A}}\mathbf{H}_{\mathrm{SA}} + \mathbf{h}_{\mathrm{SR}}\right\|}. \quad (2)$$

and the received signal-to-noise ratio (SNR) at R can be represented as

$$\gamma_{\mathrm{R}} = \frac{P_1\left\|\mathbf{h}_{\mathrm{AR}}\mathbf{\Theta}_{\mathrm{A}}\mathbf{H}_{\mathrm{SA}} + \mathbf{h}_{\mathrm{SR}}\right\|^2}{\gamma_{\mathrm{ri}} + \sigma_n^2}. \quad (3)$$

where γ_{ri} represents the residual interference power due to imperfect loop interference cancellation [17], which largely depends on the distance between the transmit and receive antenna of the relay or/and the capability of the loop interference cancellation technique [19], [20].

In the second hop, R transmits $x_{\mathrm{R}}(t)$ to both B and D, and B reflects the incident signal towards D. Therefore, the received signal at R is given by

$$y_{\mathrm{D}}(t) = \sqrt{P_2}\left(\mathbf{h}_{\mathrm{BD}}\mathbf{\Theta}_{\mathrm{B}}\mathbf{H}_{\mathrm{RB}} + \mathbf{h}_{\mathrm{RD}}\right) f_{\mathrm{R}} x_{\mathrm{R}}(t) + n_{\mathrm{D}}, \quad (4)$$

where P_2 is the transmitted powers in the second hop, $n_{\mathrm{D}} \sim \mathcal{CN}\left(0, \sigma_{\mathrm{n}}^2\right)$ is the AWGN component at D, and f_{R} is the precoder used at R that satisfies $\|f_{\mathrm{R}}\|^2 = 1$. $x_{\mathrm{R}}(t) = x_{\mathrm{S}}(t-\tau)$, with τ being the processing delay. We assume that the processing delay $\tau \geq 1$ which guarantees the receive and transmit signals at the relay terminal are uncorrelated. This is a common assumption for FD systems (e.g., see [19], [20], and [21]).

Adopting the MRT, the precoder at R is given by

$$f_{\mathrm{R}} = \frac{\left(\mathbf{h}_{\mathrm{BD}}\mathbf{\Theta}_{\mathrm{B}}\mathbf{H}_{\mathrm{RB}} + \mathbf{h}_{\mathrm{RD}}\right)^H}{\left\|\mathbf{h}_{\mathrm{BD}}\mathbf{\Theta}_{\mathrm{B}}\mathbf{H}_{\mathrm{RB}} + \mathbf{h}_{\mathrm{RD}}\right\|}. \quad (5)$$

The received SNR at D can be represented as

$$\gamma_{\mathrm{D}} = \frac{P_2\left\|\mathbf{h}_{\mathrm{BD}}\mathbf{\Theta}_{\mathrm{B}}\mathbf{H}_{\mathrm{RB}} + \mathbf{h}_{\mathrm{RD}}\right\|^2}{\sigma_n^2}, \quad (6)$$

Taking both hops into account, the ESE of the system can be expressed as

$$\begin{aligned}\mathcal{R} &= \mathbb{E}\left\{\min\left\{\log_2\left(1+\gamma_{\mathrm{R}}\right), \log_2\left(1+\gamma_{\mathrm{D}}\right)\right\}\right\} \\ &= \mathbb{E}\left\{\min\left\{\log_2\left(1+\frac{P_1\left\|\mathbf{h}_{\mathrm{AR}}\mathbf{\Theta}_{\mathrm{A}}\mathbf{H}_{\mathrm{SA}} + \mathbf{h}_{\mathrm{SR}}\right\|^2}{\gamma_{\mathrm{ri}} + \sigma_n^2}\right),\right.\right.\right. \\ &\qquad \left.\left.\left.\log_2\left(1+\frac{P_2\left\|\mathbf{h}_{\mathrm{BD}}\mathbf{\Theta}_{\mathrm{B}}\mathbf{H}_{\mathrm{RB}} + \mathbf{h}_{\mathrm{RD}}\right\|^2}{\sigma_n^2}\right)\right\}\right\}. \end{aligned} \quad (7)$$

B. CHANNEL MODEL

In this subsection, we describe the composite channel model in detail. All links are assumed to experience both small and large-scale fading. Because the channels involved in this system include outdoor, indoor, and outdoor-to-indoor, the large-scale fading of various channels should also be modeled according to the corresponding channel environments.

In this paper, we adopt the close-in free space reference distance model with frequency-dependent path loss exponent to model the large-scale fading of different links. Specifically, the large-scale fading of the outdoor/indoor links can be expressed as

$$\eta(f, d) = -20\lg\left(\frac{4\pi f}{c}\right) - 10\alpha\left(1+\beta\left(\frac{f-f_0}{f}\right)\right)\lg(d), \quad (8)$$

where f is the carrier frequency in GHz, d is the distance between two nodes, c is the speed of light, f_0 is a fixed reference frequency, α is the path loss exponent, and β is a system parameter. We adopt the "Outdoor UMi-Street Canyon" and the "Indoor Office" environments reported in [22].

The large-scale fading model of the outdoor-to-indoor link needs to consider penetration loss, which can be expressed as

$$\eta = \eta_{\mathrm{b}} + \eta_{\mathrm{t}} + \eta_{\mathrm{in}}, \tag{9}$$

where η_{b} is the basic outdoor path loss, η_{t} is the building penetration loss through the external wall, and η_{in} is the inside loss dependent on the depth into the building. Furthermore, these loss factors can be expressed as

$$\begin{cases} \eta_{\mathrm{b}} = \eta_{\mathrm{B}}\left(f, d_{\mathrm{out}} + d_{\mathrm{in}}\right) \\ \eta_{\mathrm{t}} = 14 + 15(1 - \cos(\phi))^2 \\ \eta_{\mathrm{in}} = 0.5 d_{\mathrm{in}}, \end{cases} \tag{10}$$

where $\eta_{\mathrm{B}}(f, d)$ is the basic path loss given by (8), ϕ is the angle of incidence, d_{out} and d_{in} represent the LoS transmission path length of the link from the transmitter to the wall and the indoor transmission distance of the signal, respectively.

In high frequency band communications, the channels are perhaps dominated by the LoS paths. The results in [23] also indicate that the Rician distribution can yield higher channel capacity compared to the Rayleigh assumption when the number of transmit antennas is small. To match the practical implementation, we model the channels between S $\rightarrow$ A, A $\rightarrow$ R, R $\rightarrow$ B, B $\rightarrow$ D as Rician fading according to [10], which can be written as

$$\mathbf{H}_i = \sqrt{\frac{K_i}{K_i+1}}\sqrt{\bar{\eta}_i}\bar{\mathbf{H}}_i + \sqrt{\frac{1}{K_i+1}}\sqrt{\tilde{\eta}_i}\tilde{\mathbf{H}}_i, \tag{11}$$

where K_i denotes the Rician factor, $i \in \{\mathrm{SA}, \mathrm{AR}, \mathrm{RB}, \mathrm{BD}\}$, $\bar{\mathbf{H}}_i$ and $\tilde{\mathbf{H}}_i$ contain the LoS and NLoS components, respectively, $\bar{\eta}_i$ and $\tilde{\eta}_i$ represent the large-scale fading effects of the corresponding LoS and NLoS paths, respectively. The elements of $\tilde{\mathbf{H}}_i$ are i.i.d. complex Gaussian random variables, each of which has zero mean and unit variance. On the other hand, the LoS components remain unchanged within the channel coherence time, which can be expressed by the responses of the uniform linear array (ULA) as

$$\bar{\mathbf{H}}_i = \mathbf{a}^H\left(N_{\mathrm{r},i}, \theta_{\mathrm{AoA},i}\right)\mathbf{a}\left(N_{\mathrm{t},i}, \theta_{\mathrm{AoD},i}\right). \tag{12}$$

In the above expression, the normalized array response vector of an N-element ULA is

$$\mathbf{a}(N, \theta) = \left[1, e^{j2\pi\frac{d_{\mathrm{a}}}{\lambda}\sin\theta}, \ldots, e^{j2\pi\frac{d_{\mathrm{a}}}{\lambda}(N-1)\sin\theta}\right], \tag{13}$$

where λ is the wavelength of the carrier, θ is the angle of departure (AoD) or angle of arrival (AoA) of a signal, and d_{a} is the inter-element spacing. Here we make a common assumption that $d_{\mathrm{a}} = \frac{\lambda}{2}$.

To take into account the practical scenario that the LoS paths between S $\rightarrow$ R and R $\rightarrow$ D may be blocked, we model these two propagation environments as Rayleigh fading: $\mathbf{h}_j = \sqrt{\tilde{\eta}_j}\tilde{\mathbf{h}}_j$, $j \in \{\mathrm{SR}, \mathrm{RD}\}$. Here, the elements of $\tilde{\mathbf{h}}_j$ are also i.i.d. complex Gaussian random variables with zero mean and unit variance.

III. PERFORMANCE ANALYSIS

A. UPPER BOUND OF ESE

In this subsection, we theoretically analyze the ESE of the proposed hybrid double-RIS and FD DF-relay aided system and then evaluate the effects of different propagation environments. The analysis is also helpful for designing the phase shifts and optimizing power allocation in Section IV.

First, using the Jensen's inequality $\mathbb{E}(\log(1+\gamma)) \leq \log(1+\mathbb{E}(\gamma))$, we consider the upper bound of $\mathcal{R}$ as

$$\mathcal{R}_{\mathrm{up}} = \log_2\left(1 + \min\left\{\mathbb{E}(\gamma_{\mathrm{R}}), \mathbb{E}(\gamma_{\mathrm{D}})\right\}\right). \tag{14}$$

Next, we analyze the expected value of γ_{R} and decompose $\mathbf{h}_{\mathrm{AR}}\boldsymbol{\Theta}_{\mathrm{A}}\mathbf{H}_{\mathrm{SA}}$ as (15), shown at the bottom of the page, where the first term z_1 is constant. $\tilde{\mathbf{h}}_{\mathrm{AR}}$, $\tilde{\mathbf{H}}_{\mathrm{SA}}$, and $\mathbf{h}_{\mathrm{SR}}$ have zero means and are independent with each other, so $\mathbb{E}(z_i) = 0$ holds for $i = 2, 3, 4$.

Therefore, we have

$$\begin{aligned} \mathbb{E}(\gamma_{\mathrm{R}}) &= \frac{P_1}{\gamma_{\mathrm{ri}} + \sigma_n^2}\mathbb{E}\left(\left\|\mathbf{h}_{\mathrm{AR}}\boldsymbol{\Theta}_{\mathrm{A}}\mathbf{H}_{\mathrm{SA}} + \mathbf{h}_{\mathrm{SR}}\right\|^2\right) \\ &= \frac{P_1}{\gamma_{\mathrm{ri}} + \sigma_n^2}\left(\mathbb{E}\left(\left\|\mathbf{h}_{\mathrm{AR}}\boldsymbol{\Theta}_{\mathrm{A}}\mathbf{H}_{\mathrm{SA}}\right\|^2\right) + \left(\mathbb{E}\left\|\mathbf{h}_{\mathrm{SR}}\right\|^2\right)\right) \\ &= \frac{P_1}{\gamma_{\mathrm{ri}} + \sigma_n^2}\left(\frac{\|z_1\|^2 + \mathbb{E}\left(\|z_2\|^2 + \|z_3\|^2 + \|z_4\|^2\right)}{(K_{\mathrm{AR}}+1)(K_{\mathrm{SA}}+1)}\right. \\ &\quad \left. + \mathbb{E}\left(\left\|\mathbf{h}_{\mathrm{SR}}\right\|^2\right)\right). \end{aligned} \tag{16}$$

For the channel between the S and the R, it holds that

$$\mathbb{E}\left(\left\|\mathbf{h}_{\mathrm{SR}}\right\|^2\right) = \tilde{\eta}_{\mathrm{SR}} N_{\mathrm{S}}. \tag{17}$$

$$\mathbf{h}_{\mathrm{AR}}\boldsymbol{\Theta}_{\mathrm{A}}\mathbf{H}_{\mathrm{SA}} = \frac{1}{\sqrt{(K_{\mathrm{AR}}+1)(K_{\mathrm{SA}}+1)}}\left(\underbrace{\sqrt{K_{\mathrm{AR}}K_{\mathrm{SA}}}\sqrt{\bar{\eta}_{\mathrm{AR}}\bar{\eta}_{\mathrm{SA}}}\bar{\mathbf{h}}_{\mathrm{AR}}\Theta_{\mathrm{A}}\bar{\mathbf{H}}_{\mathrm{SA}}}_{z_1} + \underbrace{\sqrt{K_{\mathrm{SA}}}\sqrt{\tilde{\eta}_{\mathrm{AR}}\bar{\eta}_{\mathrm{SA}}}\tilde{\mathbf{h}}_{\mathrm{AR}}\Theta_{\mathrm{A}}\bar{\mathbf{H}}_{\mathrm{SA}}}_{z_2}\right.$$
$$\left. + \underbrace{\sqrt{K_{\mathrm{AR}}}\sqrt{\bar{\eta}_{\mathrm{AR}}\tilde{\eta}_{\mathrm{SA}}}\bar{\mathbf{h}}_{\mathrm{AR}}\Theta_{\mathrm{A}}\tilde{\mathbf{H}}_{\mathrm{SA}}}_{z_3} + \underbrace{\sqrt{\tilde{\eta}_{\mathrm{AR}}\tilde{\eta}_{\mathrm{SA}}}\tilde{\mathbf{h}}_{\mathrm{AR}}\Theta_{\mathrm{A}}\tilde{\mathbf{H}}_{\mathrm{SA}}}_{z_4}\right) \tag{15}$$

For the other terms in (15), it can be verified that

$$\begin{aligned}\mathbb{E}\left(\|z_2\|^2\right) &= K_{\mathrm{SA}}\tilde{\eta}_{\mathrm{AR}}\bar{\eta}_{\mathrm{SA}}\rho^2 N_{\mathrm{S}}N_{\mathrm{A}},\\ \mathbb{E}\left(\|z_3\|^2\right) &= K_{\mathrm{AR}}\bar{\eta}_{\mathrm{AR}}\tilde{\eta}_{\mathrm{SA}}\rho^2 N_{\mathrm{S}}N_{\mathrm{A}},\\ \mathbb{E}\left(\|z_4\|^2\right) &= \tilde{\eta}_{\mathrm{AR}}\tilde{\eta}_{\mathrm{SA}}\rho^2 N_{\mathrm{S}}N_{\mathrm{A}}.\end{aligned} \tag{18}$$

Thus, by substituting (17) and (18) into (16), we obtain the expected value of the received SNR at R as follows:

$$\mathbb{E}\left(\gamma_{\mathrm{R}}\right) = \frac{P_1\left(\mathcal{K}_1\left\|\bar{\mathbf{h}}_{\mathrm{AR}}\boldsymbol{\Theta}_{\mathrm{A}}\bar{\mathbf{H}}_{\mathrm{SA}}\right\|^2 + \mathcal{K}_2\rho^2 N_{\mathrm{S}}N_{\mathrm{A}} + \tilde{\eta}_{\mathrm{SR}}N_{\mathrm{S}}\right)}{\gamma_{\mathrm{ri}} + \sigma_n^2}. \tag{19}$$

where

$$\begin{aligned}\mathcal{K}_1 &= \frac{K_{\mathrm{AR}}K_{\mathrm{SA}}\bar{\eta}_{\mathrm{AR}}\bar{\eta}_{\mathrm{SA}}}{\left(K_{\mathrm{AR}}+1\right)\left(K_{\mathrm{SA}}+1\right)},\\ \mathcal{K}_2 &= \frac{K_{\mathrm{SA}}\tilde{\eta}_{\mathrm{AR}}\bar{\eta}_{\mathrm{SA}} + K_{\mathrm{AR}}\bar{\eta}_{\mathrm{AR}}\tilde{\eta}_{\mathrm{SA}} + \tilde{\eta}_{\mathrm{AR}}\tilde{\eta}_{\mathrm{SA}}}{\left(K_{\mathrm{AR}}+1\right)\left(K_{\mathrm{SA}}+1\right)}.\end{aligned} \tag{20}$$

Similarly, we can obtain the expected value of the received SNR at D as

$$\mathbb{E}\left(\gamma_{\mathrm{D}}\right) = \frac{P_2\left(\mathcal{K}_3\left\|\bar{\mathbf{h}}_{\mathrm{BD}}\boldsymbol{\Theta}_{\mathrm{B}}\bar{\mathbf{H}}_{\mathrm{RB}}\right\|^2 + \mathcal{K}_4\rho^2 N_{\mathrm{R}}N_{\mathrm{B}} + \tilde{\eta}_{\mathrm{RD}}N_{\mathrm{R}}\right)}{\sigma_n^2}, \tag{21}$$

where

$$\begin{aligned}\mathcal{K}_3 &= \frac{K_{\mathrm{BD}}K_{\mathrm{RB}}\bar{\eta}_{\mathrm{BD}}\bar{\eta}_{\mathrm{RB}}}{\left(K_{\mathrm{BD}}+1\right)\left(K_{\mathrm{RB}}+1\right)},\\ \mathcal{K}_4 &= \frac{K_{\mathrm{BD}}\bar{\eta}_{\mathrm{BD}}\tilde{\eta}_{\mathrm{RB}} + K_{\mathrm{RB}}\tilde{\eta}_{\mathrm{BD}}\bar{\eta}_{\mathrm{RB}} + \tilde{\eta}_{\mathrm{BD}}\tilde{\eta}_{\mathrm{RB}}}{\left(K_{\mathrm{BD}}+1\right)\left(K_{\mathrm{RB}}+1\right)}.\end{aligned} \tag{22}$$

Finally, the upper bound of the ESE can be computed as

$$\mathcal{R}_{\mathrm{up}} = \log_2\left(1 + \min\left\{\frac{P_1\gamma_1}{\gamma_{\mathrm{ri}}+\sigma_n^2}, \frac{P_2\gamma_2}{\sigma_n^2}\right\}\right). \tag{23}$$

where the newly-introduced parameters γ_1 and γ_2 are given by

$$\gamma_1 = \mathcal{K}_1\left\|\bar{\mathbf{h}}_{\mathrm{AR}}\boldsymbol{\Theta}_{\mathrm{A}}\bar{\mathbf{H}}_{\mathrm{SA}}\right\|^2 + \mathcal{K}_2\rho^2 N_{\mathrm{S}}N_{\mathrm{A}} + \tilde{\eta}_{\mathrm{SR}}N_{\mathrm{S}}, \tag{24}$$

$$\gamma_2 = \mathcal{K}_3\left\|\bar{\mathbf{h}}_{\mathrm{BD}}\boldsymbol{\Theta}_{\mathrm{B}}\bar{\mathbf{H}}_{\mathrm{RB}}\right\|^2 + \mathcal{K}_4\rho^2 N_{\mathrm{R}}N_{\mathrm{B}} + \tilde{\eta}_{\mathrm{RD}}N_{\mathrm{R}}. \tag{25}$$

B. EFFECTS OF RICIAN-K FACRORS AND PHASE SHIFTS

In order to understand the influence of the channel conditions and the passive beamforming of the RISs on the performance, we investigate different channel Rician-K factors in this subsection. We consider the following cases.

Case 1: If $K_{\mathrm{SA}}K_{\mathrm{AR}} = 0$, i.e., at least one of the channels between S and A and between A and R is Rayleigh fading caused by the blockage in the LoS path, the expected value of the received SNR at R is

$$\mathbb{E}\left(\gamma_{\mathrm{R}}\right) = \frac{P_1}{\gamma_{\mathrm{ri}}+\sigma_n^2}\left(\tilde{\eta}_{\mathrm{AR}}\tilde{\eta}_{\mathrm{SA}}\rho^2 N_{\mathrm{S}}N_{\mathrm{A}} + \tilde{\eta}_{\mathrm{SR}}N_{\mathrm{S}}\right). \tag{26}$$

Similarly, if $K_{\mathrm{BD}}K_{\mathrm{RB}} = 0$, i.e., at least one of the channels between B and D and between R and B is Rayleigh fading, the expected value of the received SNR at D is

$$\mathbb{E}\left(\gamma_{\mathrm{D}}\right) = \frac{P_2}{\sigma_n^2}\left(\tilde{\eta}_{\mathrm{BD}}\tilde{\eta}_{\mathrm{RB}}\rho^2 N_{\mathrm{R}}N_{\mathrm{B}} + \tilde{\eta}_{\mathrm{RD}}N_{\mathrm{R}}\right). \tag{27}$$

Then the ESE of the system is upper bounded by

$$\mathcal{R}_{\mathrm{up}} = \log_2\left(1 + \min\left\{\frac{P_1\left(\tilde{\eta}_{\mathrm{AR}}\tilde{\eta}_{\mathrm{SA}}\rho^2 N_{\mathrm{S}}N_{\mathrm{A}} + \tilde{\eta}_{\mathrm{SR}}N_{\mathrm{S}}\right)}{\gamma_{\mathrm{ri}}+\sigma_n^2}, \frac{P_2\left(\tilde{\eta}_{\mathrm{BD}}\tilde{\eta}_{\mathrm{RB}}\rho^2 N_{\mathrm{R}}N_{\mathrm{B}} + \tilde{\eta}_{\mathrm{RD}}N_{\mathrm{R}}\right)}{\sigma_n^2}\right\}\right). \tag{28}$$

We observe that in Case 1, $\mathcal{R}_{\mathrm{up}}$ is independent of $\boldsymbol{\Theta}_{\mathrm{A}}$ and $\boldsymbol{\Theta}_{\mathrm{B}}$. This phenomenon is caused by the spatial isotropy of the assisting channel, which is insensitive to the beamforming operations performed at RIS A and RIS B.

Case 2: If $K_i \to \infty,\ i \in \{\mathrm{SA}, \mathrm{AR}, \mathrm{RB}, \mathrm{BD}\}$, then the upper bound of the ESE can be obtained as (29). In this case, only LoS components exist, and the assisting channels remain unchanged. Thus, the ESE of the system is sensitive to passive beamforming design at RIS A and RIS B.

$$\mathcal{R}_{\mathrm{up}} = \log_2\left(1 + \min\left\{\frac{P_1\left(\left\|\bar{\mathbf{h}}_{\mathrm{AR}}\boldsymbol{\Theta}_{\mathrm{A}}\bar{\mathbf{H}}_{\mathrm{SA}}\right\|^2 + \tilde{\eta}_{\mathrm{SR}}N_{\mathrm{S}}\right)}{\gamma_{\mathrm{ri}}+\sigma_n^2}, \frac{P_2\left(\left\|\bar{\mathbf{h}}_{\mathrm{BD}}\boldsymbol{\Theta}_{\mathrm{B}}\bar{\mathbf{H}}_{\mathrm{RB}}\right\|^2 + \tilde{\eta}_{\mathrm{RD}}N_{\mathrm{R}}\right)}{\sigma_n^2}\right\}\right). \tag{29}$$

C. COMPARISION BETWEEN HD AND FD MODES

In this subsection, we investigate the impact of using HD and FD relays on the performance of the proposed system under antenna preserved - same number of transmit / receive antennas. First, it requires two orthogonal time slots for transmission in the HD mode: S to R and R to D [24]. Second, the HD mode does not induce loop interference. Therefore, the spectral efficiency of the system in the HD mode can be obtained directly from (3) and (6) by neglecting the loop interference effect. Third, with the HD mode, S and R transmit only half of the time as compared to the FD mode. As such there is a pre-log factor of 1/2 in the expression of spectral efficiency. Furthermore, to ensure that the transmitted powers spent in a coherence interval for both modes are same, the transmitted powers of S and R used in the HD mode are twice of that used in the FD mode.

Then, with the HD mode, the received signal of the first hop can be given as

$$\gamma_{\mathrm{R}}^{\mathrm{HD}} = \frac{2P_1\left\|\mathbf{h}_{\mathrm{AR}}\boldsymbol{\Theta}_{\mathrm{A}}\mathbf{H}_{\mathrm{SA}} + \mathbf{h}_{\mathrm{SR}}\right\|^2}{\sigma_n^2}. \tag{30}$$

The received signal of the second hop is

$$\gamma_{\mathrm{D}}^{\mathrm{HD}} = \frac{2P_2\left\|\mathbf{h}_{\mathrm{BD}}\boldsymbol{\Theta}_{\mathrm{B}}\mathbf{H}_{\mathrm{RB}} + \mathbf{h}_{\mathrm{RD}}\right\|^2}{\sigma_n^2}. \tag{31}$$

Therefore, the ESE of the system with the HD relay is given as follows:

$$\mathcal{R}^{\mathrm{HD}} = \mathbb{E}\left\{\frac{1}{2}\log_2\left(1+\min\left\{\gamma_{\mathrm{R}}^{\mathrm{HD}},\gamma_{\mathrm{D}}^{\mathrm{HD}}\right\}\right)\right\} \le \frac{1}{2}\log_2\left(1+\min\left\{\frac{2P_1\gamma_1}{\sigma_n^2},\frac{2P_2\gamma_2}{\sigma_n^2}\right\}\right). \quad (32)$$

Moreover, the HD and FD modes are also slightly different in terms of energy efficiency. To define the EEE metric, we first provide the description of the power consumption models. The total power consumption is composed of the transmit power of S and R, the hardware static power consumed in S, R, D, and the RISs [25], [26]. With the above explanation of the power consumption, the total power consumption of the HD mode can be expressed as

$$P_{\mathrm{tot}}^{\mathrm{HD}} = \beta_{\mathrm{a}}(P_1+P_2) + P_{\mathrm{c}}^{\mathrm{S}} + P_{\mathrm{c}}^{\mathrm{R}} + 2P_{\mathrm{c}}^{\mathrm{D}} + (N_{\mathrm{A}}+N_B)P_n(b) + (N_{\mathrm{S}}+N_{\mathrm{R}})P_{\mathrm{A}}. \quad (33)$$

where $\beta_{\mathrm{a}} = v^{-1}$ with $0 < v < 1$ being the efficiency of the transmit power amplifier at S and R. $P_{\mathrm{c}}^{\mathrm{S}}$, $P_{\mathrm{c}}^{\mathrm{R}}$, and $P_{\mathrm{c}}^{\mathrm{D}}$ are the hardware static power consumption at S, R, and D, respectively. $P_n(b)$ denotes the power consumption of each phase shifter having b-bit resolution at an identical reflecting element. P_{A} denotes dissipated power of each active antenna.

The FD mode needs to consume a certain amount of energy for self-interference cancellation (SIC), defined here as P_{SIC} [27]. P_{SIC} is modeled as a linear function over the transmission power P_2, which can be determined by

$$P_{\mathrm{SIC}} = \beta_{\mathrm{s}}\beta_{\mathrm{a}}P_2 + P_{c0}. \quad (34)$$

where β_{s} is the isolation factor and $\beta_{\mathrm{s}}P_2$ denotes a part of the relay transmission power, which is used for self-interference signal reconstruction. P_{c0} is the sum of analogy cancellation power consumption and digital cancellation power consumption except for power amplifier power consumption. Then we can obtain the total power consumption of the FD mode, i.e.,

$$P_{\mathrm{tot}}^{\mathrm{FD}} = \beta_{\mathrm{a}}(P_1+P_2) + P_{\mathrm{c}}^{\mathrm{S}} + P_{\mathrm{c}}^{\mathrm{R}} + P_{\mathrm{c}}^{\mathrm{D}} + P_{\mathrm{SIC}} + (N_{\mathrm{A}}+N_B)P_n(b) + (N_{\mathrm{S}}+N_{\mathrm{R}})P_{\mathrm{A}}. \quad (35)$$

According to the characterizations of the ESE and the power consumption models, the EEE of FD and HD modes can be defined as $\eta_{\mathrm{E}}^{\mathrm{FD}} = W\mathcal{R}/P_{\mathrm{tot}}^{\mathrm{FD}}$ and $\eta_{\mathrm{E}}^{\mathrm{HD}} = W\mathcal{R}^{\mathrm{HD}}/P_{\mathrm{tot}}^{\mathrm{HD}}$, respectively, where W is the transmission bandwidth.

IV. PASSIVE BEAMFORMING DESIGN AND OPTIMIZATION OF POWER ALLOCATION

In this paper, we focus on maximizing the ESE by jointly optimizing the passive beamforming. By formula derivation in section III, we turn to maximizing the upper bound $\mathcal{R}_{\mathrm{up}}$ to achieve the same purpose. When the transmitted powers, Rician-K factors, and the number of antennas/elements are fixed, the corresponding optimization problem can be formulated as

$$\mathcal{P}(a)\ \max_{\boldsymbol{\Theta}_{\mathrm{A}},\boldsymbol{\Theta}_{\mathrm{B}}}\ \mathcal{R}_{\mathrm{up}} = \log_2\left(1+\min\left\{\frac{P_1\gamma_1}{\gamma_{\mathrm{ri}}+\sigma_n^2},\frac{P_2\gamma_2}{\sigma_n^2}\right\}\right)$$
$$\text{s.t.}\quad 0<\varphi(\mathrm{A},n)\le 2\pi, \forall n=1,\cdots,N_{\mathrm{A}}$$
$$0<\varphi(\mathrm{B},n)\le 2\pi, \forall n=1,\cdots,N_{\mathrm{B}}. \quad (36)$$

Maximizing the upper bound $\mathcal{R}_{\mathrm{up}}$ is equivalent to maximizing the minimum of γ_1 and γ_2. According to (24) and (25), γ_1 and γ_2 depend on $\left\|\bar{\mathbf{h}}_{\mathrm{AR}}\boldsymbol{\Theta}_{\mathrm{A}}\bar{\mathbf{H}}_{\mathrm{SA}}\right\|^2$ and $\left\|\bar{\mathbf{h}}_{\mathrm{BD}}\boldsymbol{\Theta}_{\mathrm{B}}\bar{\mathbf{H}}_{\mathrm{RB}}\right\|^2$, respectively. However, they are independent of each other. The problem of maximizing the minimum can be converted to maximizing them simultaneously to design the passive beamforming, i.e., $\boldsymbol{\Theta}_{\mathrm{A}}$ and $\boldsymbol{\Theta}_{\mathrm{B}}$ can be designed by maximizing $\left\|\bar{\mathbf{h}}_{\mathrm{AR}}\boldsymbol{\Theta}_{\mathrm{A}}\bar{\mathbf{H}}_{\mathrm{SA}}\right\|^2$ and $\left\|\bar{\mathbf{h}}_{\mathrm{BD}}\boldsymbol{\Theta}_{\mathrm{B}}\bar{\mathbf{H}}_{\mathrm{RB}}\right\|^2$, respectively.

In this section, we first propose two methods for optimizing $\boldsymbol{\Theta}_{\mathrm{A}}$ and $\boldsymbol{\Theta}_{\mathrm{B}}$, which are suitable for continuous and discrete phase shifts, respectively. Then we design an OPA scheme to further enhance the performance.

A. DESIGN OF CONTINUOUS PHASE SHIFTS – OPS

In the case of continuous phase shifts, the range of phase shift is $(0, 2\pi]$. Therefore, we can obtain the OPS solutions by solving the following two subproblems

$$\mathcal{P}(b1)\ \max_{\boldsymbol{\Theta}_{\mathrm{A}}}\ \left\|\bar{\mathbf{h}}_{\mathrm{AR}}\boldsymbol{\Theta}_{\mathrm{A}}\bar{\mathbf{H}}_{\mathrm{SA}}\right\|^2 \quad \text{s.t.}\ 0<\varphi(\mathrm{A},n)\le 2\pi, \forall n=1,\cdots,N_{\mathrm{A}}. \quad (37)$$

$$\mathcal{P}(b2)\ \max_{\boldsymbol{\Theta}_{\mathrm{B}}}\ \left\|\bar{\mathbf{h}}_{\mathrm{BD}}\boldsymbol{\Theta}_{\mathrm{B}}\bar{\mathbf{H}}_{\mathrm{RB}}\right\|^2 \quad \text{s.t.}\ 0<\varphi(\mathrm{B},n)\le 2\pi, \forall n=1,\cdots,N_{\mathrm{B}}. \quad (38)$$

First, for the optimal $\boldsymbol{\Theta}_{\mathrm{A,OPS}} = \max_{\boldsymbol{\Theta}_{\mathrm{A}}}\left\|\bar{\mathbf{h}}_{\mathrm{AR}}\boldsymbol{\Theta}_{\mathrm{A}}\bar{\mathbf{H}}_{\mathrm{SA}}\right\|^2$, we introduce a new variable ε_{A} as

$$\varepsilon_{\mathrm{A}} = \mathbf{a}(N_{\mathrm{A}},\theta_{\mathrm{AR}})\boldsymbol{\Theta}_{\mathrm{A}}\mathbf{a}^H\left(N_{\mathrm{A}},\theta_{\mathrm{AoA,SA}}\right) = \sum_{n=1}^{N_{\mathrm{A}}}\rho e^{j2\pi\frac{d_{\mathrm{a}}}{\lambda}(n-1)\left(\sin\theta_{\mathrm{AR}}-\sin\theta_{\mathrm{AoA,SA}}\right)+j\varphi(\mathrm{A},n)}, \quad (39)$$

where θ_{AR} is the AoD of the channel from A to R and $\theta_{\mathrm{AoA,SA}}$ is the AoA of the channel from S to A.

Then the optimal value of $\boldsymbol{\Theta}_{\mathrm{A}}$ can be converted to $\boldsymbol{\Theta}_{\mathrm{A,OPS}} = \max_{\boldsymbol{\Theta}_{\mathrm{A}}}|\varepsilon_{\mathrm{A}}|^2\left\|\mathbf{a}\left(N_{\mathrm{S}},\theta_{\mathrm{AoD,SA}}\right)\right\|^2$, where $\theta_{\mathrm{AoD,SA}}$ is the AoD of the channel from S to A and $\left\|\mathbf{a}\left(N_{\mathrm{S}},\theta_{\mathrm{AoD,SA}}\right)\right\|^2 = N_{\mathrm{S}}$ is a constant. Hence, the optimal phase shifts can also be obtained by maximizing $|\varepsilon_{\mathrm{A}}|^2$, of which the maximum is $\rho^2N_{\mathrm{A}}^2$. For the case of random phase shift used on each element of A, i.e., $\varphi(\mathrm{A},n)$ is randomly distributed in $(0, 2\pi]$. It does not affect the distribution of $(\sin\theta_{\mathrm{AR}} - \sin\theta_{\mathrm{AoA,SA}})$. So $|\varepsilon_{\mathrm{A}}|^2 = \rho^2N_{\mathrm{A}}$ when the RIS A adopt the random phases.

ε_{A} can reach the maximum value only if the phases of A are adjusted to make the signal be received coherently. The optimum solution for the n-th reflecting element of A is

$$\varphi^{\mathrm{opt}}(\mathrm{A},n) = 2\pi\frac{d_{\mathrm{a}}}{\lambda}(n-1)\left(\sin\theta_{\mathrm{AoA,SA}}-\sin\theta_{\mathrm{AR}}\right). \quad (40)$$

Then the expected value of the received SNR in the first hop with the OPS solution can be expressed as

$$\mathbb{E}\left(\gamma_{\mathrm{R,OPS}}\right) = \frac{P_1\left(\mathcal{K}_1\rho^2N_{\mathrm{A}}^2N_{\mathrm{S}} + \mathcal{K}_2\rho^2N_{\mathrm{A}}N_{\mathrm{S}} + \tilde{\eta}_{\mathrm{SR}}N_{\mathrm{S}}\right)}{\gamma_{\mathrm{ri}}+\sigma_n^2}. \quad (41)$$

For the optimal $\mathbf{\Theta}_{\mathrm{B,\,OPS}} = \max_{\mathbf{\Theta}_{\mathrm{B}}} \left\| \bar{\mathbf{h}}_{\mathrm{BD}} \mathbf{\Theta}_{\mathrm{B}} \bar{\mathbf{H}}_{\mathrm{RB}} \right\|^2$, we introduce a new variable ε_{B} as

$$\begin{aligned} \varepsilon_{\mathrm{B}} &= \mathbf{a}\left(N_{\mathrm{B}}, \theta_{\mathrm{BD}}\right) \mathbf{\Theta}_{\mathrm{B}} \mathbf{a}^{H}\left(N_{\mathrm{B}}, \theta_{\mathrm{AOA,\,RB}}\right) \\ &= \sum_{n=1}^{N_{\mathrm{B}}} \rho e^{j2\pi \frac{d_{\mathrm{a}}}{\lambda}(n-1)\left(\sin\theta_{\mathrm{BD}} - \sin\theta_{\mathrm{AOA,\,RB}}\right) + j\varphi(\mathrm{B},n)}. \end{aligned} \tag{42}$$

Similarly, we can obtain that $|\varepsilon_{\mathrm{B}}|^2 = \rho^2 N_{\mathrm{B}}$ when the RIS B adopts the random phases.

Then, the optimum solution for the n-th reflecting element at B is

$$\varphi^{\mathrm{opt}}(\mathrm{B}, n) = 2\pi \frac{d_{\mathrm{a}}}{\lambda}(n-1)\left(\sin\theta_{\mathrm{AOA,\,RB}} - \sin\theta_{\mathrm{BD}}\right). \tag{43}$$

We have $|\varepsilon_{\mathrm{B}}|^2 = \rho^2 N_{\mathrm{B}}^2$ and the expected value of the received SNR in the second hop with the OPS can be expressed as

$$\mathbb{E}\left(\gamma_{\mathrm{D,OPS}}\right) = \frac{P_2\left(\mathcal{K}_3 \rho^2 N_{\mathrm{B}}^2 N_{\mathrm{R}} + \mathcal{K}_4 \rho^2 N_{\mathrm{B}} N_{\mathrm{R}} + \tilde{\eta}_{\mathrm{RD}} N_{\mathrm{R}}\right)}{\sigma_n^2}. \tag{44}$$

Finally, the ESE of the system with the OPS is upper bounded by (45), as shown at the bottom of the page.

Meanwhile, we can obtain an upper bound on the ESE with the random phases as (46), shown at the bottom of the page.

B. DESIGN OF DISCRETE PHASE SHIFTS – GCE

Tuning the phase shift of each element of the RISs continuously is costly to implement in practice. The reason is that manufacturing such high-precision elements requires expensive hardware if the number of elements is very large. In this subsection, we consider a practical configuration in which the RISs are controlled by a finite number of discrete adjustable phase shifts. If the number of quantization bits is b, the phase shifts can only take values in the set $\mathcal{F} = \left\{0, \frac{2\pi}{2^b}, \cdots, \frac{2\pi}{2^b}\left(2^b - 1\right)\right\}$. The discrete phase shifts can be optimized by solving the following two subproblems

$$\begin{aligned} \mathcal{P}(c1) \quad & \max_{\mathbf{\Theta}_{\mathrm{A}}} \left\| \bar{\mathbf{h}}_{\mathrm{AR}} \mathbf{\Theta}_{\mathrm{A}} \bar{\mathbf{H}}_{\mathrm{SA}} \right\|^2 \\ & \text{s.t.} \quad \varphi(\mathrm{A}, n) \in \mathcal{F}, \forall n = 1, \cdots, N_{\mathrm{A}}, \end{aligned} \tag{47}$$

$$\begin{aligned} \mathcal{P}(c2) \quad & \max_{\mathbf{\Theta}_{\mathrm{B}}} \left\| \bar{\mathbf{h}}_{\mathrm{BD}} \mathbf{\Theta}_{\mathrm{B}} \bar{\mathbf{H}}_{\mathrm{RB}} \right\|^2 \\ & \text{s.t.} \quad \varphi(\mathrm{B}, n) \in \mathcal{F}, \forall n = 1, \cdots, N_{\mathrm{B}}. \end{aligned} \tag{48}$$

In the existing literature [28], [29], a common way of discrete beamforming is to round the relaxed continuous solution in (40) and (43) to the closest point in the discrete set, referred to as the Closest Point Projection (CPP) algorithm. However, the algorithm is heuristic and the performance cannot be guaranteed theoretically.

Then we propose a GCE algorithm for optimizing $\mathbf{\Theta}_{\mathrm{A}}$ and $\mathbf{\Theta}_{\mathrm{B}}$ to maximize $\left\| \bar{\mathbf{h}}_{\mathrm{AR}} \mathbf{\Theta}_{\mathrm{A}} \bar{\mathbf{H}}_{\mathrm{SA}} \right\|^2$ and $\left\| \bar{\mathbf{h}}_{\mathrm{BD}} \mathbf{\Theta}_{\mathrm{B}} \bar{\mathbf{H}}_{\mathrm{RB}} \right\|^2$. The GCE algorithm can be considered as a revised version of the CE algorithm developed from machine learning [30]. The pseudo-code of the proposed GCE algorithm is summarized in Algorithm 1 and explained further below.

We first describe the optimization process for $\mathbf{\Theta}_{\mathrm{A}}$ in detail. At the beginning, we define the probability matrix as $\boldsymbol{\mu}_{\mathrm{A}} \in \mathbb{C}^{2^b \times N_{\mathrm{A}}}$. The element $\mu_{\mathrm{A},l,n} \in [0, 1]$ is the probability for $\varphi(\mathrm{A}, n) = \mathcal{F}(l)$, where $\mathcal{F}(l)$ is the l-th element of $\mathcal{F}$. Note that $\sum_{l=1}^{2^b} \mu_{\mathrm{A},l,n} = 1$. In addition, we introduce a variable $\xi_{\mathrm{A}} \triangleq \left\| \bar{\mathbf{h}}_{\mathrm{AR}} \mathbf{\Theta}_{\mathrm{A}} \bar{\mathbf{H}}_{\mathrm{SA}} \right\|^2$.

We initialize $\boldsymbol{\mu}_{\mathrm{A}}^{(0)} = \frac{1}{2^b} \times 1_{2^b \times N_{\mathrm{A}}}$ (1 is the all-one matrix). The superscript of $\boldsymbol{\mu}_{\mathrm{A}}$ refers to the number of iterations of the algorithm. In Step 1, we first generate M candidate beamforming matrices $\left\{\mathbf{\Theta}_{\mathrm{A},m}\right\}_{m=1}^{M}$ based on the probability distribution $\Xi\left(\mathbf{\Theta}_{\mathrm{A}}; \boldsymbol{\mu}_{\mathrm{A}}^{(i)}\right)$, i.e., generate $\left\{\mathbf{\Theta}_{\mathrm{A},m}\right\}_{m=1}^{M}$ from $\mathcal{F}$ according to $\boldsymbol{\mu}_{\mathrm{A}}^{(i)}$. The distribution function $\Xi\left(\mathbf{\Theta}_{\mathrm{A}}; \boldsymbol{\mu}_{\mathrm{A}}^{(i)}\right)$ can be expressed as (49), shown at the bottom of the page, which is different from that in [31] using a traditional CE algorithm.

Besides, $\Omega\left(\varphi(\mathrm{A}, n), \mathcal{F}(l)\right)$ is the judge function that can be written as

$$\Omega\left(\varphi(\mathrm{A}, n), \mathcal{F}(l)\right) = \begin{cases} 1, & \varphi(\mathrm{A}, n) = \mathcal{F}(l) \\ 0, & \varphi(\mathrm{A}, n) \neq \mathcal{F}(l). \end{cases} \tag{50}$$

$$R_{\mathrm{up,OPS}} = \log_2\left\{1 + \min\left\{\frac{P_1\left(K_1 \rho^2 N_{\mathrm{A}}^2 N_{\mathrm{S}} + K_2 \rho^2 N_{\mathrm{A}} N_{\mathrm{S}} + \tilde{\eta}_{\mathrm{SR}} N_{\mathrm{S}}\right)}{\gamma_{\mathrm{ri}} + \sigma_n^2}, \frac{P_2\left(K_3 \rho^2 N_{\mathrm{B}}^2 N_{\mathrm{R}} + K_4 \rho^2 N_{\mathrm{B}} N_{\mathrm{R}} + \tilde{\eta}_{\mathrm{RD}} N_{\mathrm{R}}\right)}{\sigma_n^2}\right\}\right\} \tag{45}$$

$$R_{\mathrm{up,random}} = \log_2\left\{1 + \min\left\{\frac{P_1\left(\left(K_1 + K_2\right) \rho^2 N_{\mathrm{A}} N_{\mathrm{S}} + \tilde{\eta}_{\mathrm{SR}} N_{\mathrm{S}}\right)}{\gamma_{\mathrm{ri}} + \sigma_n^2}, \frac{P_2\left(\left(K_3 + K_4\right) \rho^2 N_{\mathrm{B}} N_{\mathrm{R}} + \tilde{\eta}_{\mathrm{RD}} N_{\mathrm{R}}\right)}{\sigma_n^2}\right\}\right\} \tag{46}$$

$$\Xi\left(\mathbf{\Theta}_{\mathrm{A}}; \boldsymbol{\mu}_{\mathrm{A}}^{(i)}\right) = \prod_{n=1}^{N}\left(\left(\prod_{l=1}^{2^b-1}\left(\mu_{\mathrm{A},l,n}^{(i)}\right)^{\Omega(\varphi(\mathrm{A},n),\mathcal{F}(l))}\right) \times \left(1 - \sum_{l=1}^{2^b-1}\left(\mu_{\mathrm{A},l,n}^{(i)}\right)\right)^{\prod_{l=1}^{2^b-1}\left(1-\Omega(\varphi(\mathrm{A},n),\mathcal{F}(l))\right)}\right) \tag{49}$$

Algorithm 1 The Proposed GCE Algorithm

Input: Channels $\bar{\mathbf{h}}_{\mathrm{AR}}$, $\bar{\mathbf{H}}_{\mathrm{SA}}$, $\bar{\mathbf{h}}_{\mathrm{BD}}$, $\bar{\mathbf{H}}_{\mathrm{RB}}$. The number of iterations I.

Initialization: $\boldsymbol{\mu}_{\mathrm{A}}^{(0)} = \frac{1}{2^b} \times 1_{2^b \times N_{\mathrm{A}}}$ and $\boldsymbol{\mu}_{\mathrm{B}}^{(0)} = \frac{1}{2^b} \times 1_{2^b \times N_{\mathrm{B}}}$.

for $i = 1, \cdots, I$ **do**

for $m = 1, \cdots, M$ **do**

1. Generate $\boldsymbol{\Theta}_{\mathrm{A},m}$ and $\boldsymbol{\Theta}_{\mathrm{B},m}$ with elements chosen from $\mathcal{F}$ randomly based on $\boldsymbol{\mu}_{\mathrm{A}}^{(i)}$ and $\boldsymbol{\mu}_{\mathrm{B}}^{(i)}$, respectively.
2. Calculate $\xi_{\mathrm{A},m}$ and $\xi_{\mathrm{B},m}$ with $\boldsymbol{\Theta}_{\mathrm{A},m}$ and $\boldsymbol{\Theta}_{\mathrm{B},m}$.

end for

3. Sort $\left\{\xi_{\mathrm{A},m}\right\}_{m=1}^{M}$ and $\left\{\xi_{\mathrm{B},m}\right\}_{m=1}^{M}$ in a descend order and select the first M_{e} optimal values as the elites.
4. Compare $\left\{\xi_{\mathrm{A},m}\right\}_{m=1}^{M_{\mathrm{e}}}$ and $\left\{\xi_{\mathrm{B},m}\right\}_{m=1}^{M}$ with the historical elites in the last iteration and update the elites by choosing the better respectively.

for $m = 1, \cdots, M_{\mathrm{e}}$ **do**

5. Calculate the weight $\omega_{\mathrm{A},m}$ for $\boldsymbol{\Theta}_{\mathrm{A},m}$ and the weight $\omega_{\mathrm{B},m}$ for $\boldsymbol{\Theta}_{\mathrm{B},m}$.

end for

6. Update $\mu_{\mathrm{A},l,n}^{(i+1)}$ based on (55) and $\mu_{\mathrm{B},l,n}^{(i+1)}$ in a similar way.

end for

Output: $\boldsymbol{\Theta}_{\mathrm{A}}^{\mathrm{opt}}$ and $\boldsymbol{\Theta}_{\mathrm{B}}^{\mathrm{opt}}$.

In Step 2, with $\left\{\boldsymbol{\Theta}_{\mathrm{A},m}\right\}_{m=1}^{M}$, we can calculate the corresponding $\left\{\xi_{\mathrm{A},m}\right\}_{m=1}^{M}$. We sort $\left\{\xi_{\mathrm{A},m}\right\}_{m=1}^{M}$ in a descending order in Step 3. Then, the elites can be obtained by choosing the first $M_{\mathrm{e}} = M/10$ optimal values. We compare the "current elite samples" with the historical elites and choose the better as the i - th iteration "global elite samples" in Step 4. This is also different compared with the conventional CE algorithm.

The next step is to update $\boldsymbol{\mu}_{\mathrm{A}}^{(i+1)}$ by minimizing the CE, which can be written as

$$\boldsymbol{\mu}_{\mathrm{A}}^{(i+1)} = \arg \max_{\boldsymbol{\mu}_{\mathrm{A}}^{(i)}} \frac{1}{M_{\mathrm{e}}} \sum_{m=1}^{M_{\mathrm{e}}} \ln \Xi\left(\boldsymbol{\Theta}_{\mathrm{A},m}; \boldsymbol{\mu}_{\mathrm{A}}^{(i)}\right). \quad (51)$$

Similar to [30], we proposed to weight each elite to increase the probability of having elites with better objective values. Specifically, we first define the auxiliary parameter T_{A} presenting the average value of $\left\{\xi_{\mathrm{A},m}\right\}_{m=1}^{M_{\mathrm{e}}}$ as

$$T_{\mathrm{A}} = \frac{1}{M_{\mathrm{e}}} \sum_{m=1}^{M_{\mathrm{e}}} \xi_{\mathrm{A},m}. \quad (52)$$

Then in Step 5, we calculate the weight $\omega_{\mathrm{A},m} = \xi_{\mathrm{A},m}/T_{\mathrm{A}}$ of the elite $\boldsymbol{\Theta}_{\mathrm{A},m}$. Based on $\left\{\omega_{\mathrm{A},m}\right\}_{m=1}^{M_{\mathrm{e}}}$, (51) can be rewritten as

$$\boldsymbol{\mu}_{\mathrm{A}}^{(i+1)} = \arg \max_{\boldsymbol{\mu}_{\mathrm{A}}^{(i)}} \frac{1}{M_{\mathrm{e}}} \sum_{m=1}^{M_{\mathrm{e}}} \omega_{\mathrm{A},m} \ln \Xi\left(\boldsymbol{\Theta}_{\mathrm{A},m}; \boldsymbol{\mu}_{\mathrm{A}}^{(i)}\right). \quad (53)$$

Substituting (49) into (53), we can obtain the first derivative of the objective function with respect to $\varphi^{(i)}(\mathrm{A}, n)$ and $\mathcal{F}(l)$ in (54), as shown at the bottom of the page.

Setting (54) to zero, $\mu_{\mathrm{A},l,n}^{(i+1)}$ can be updated in Step 6 as

$$\mu_{\mathrm{A},l,n}^{(i+1)} = \frac{\sum_{m=1}^{M_{\mathrm{e}}} \omega_{\mathrm{A},m}^{(i)} \Omega\left(\varphi^{(i)}(\mathrm{A}, n), \mathcal{F}(l)\right)}{\sum_{m=1}^{M_{\mathrm{e}}} \omega_{\mathrm{A},m}^{(i)}}. \quad (55)$$

Then introducing a variable $\xi_{\mathrm{B}} \triangleq \left\|\bar{\mathbf{h}}_{\mathrm{BD}} \boldsymbol{\Theta}_{\mathrm{B}} \bar{\mathbf{H}}_{\mathrm{RD}}\right\|^2$, the probability matrix $\boldsymbol{\mu}_{\mathrm{B}}^{(i)}$, probability distribution function $\Xi\left(\boldsymbol{\Theta}_{\mathrm{B}}; \boldsymbol{\mu}_{\mathrm{B}}^{(i)}\right)$, and the weight $\left\{\omega_{\mathrm{B},m}\right\}_{m=1}^{M_{\mathrm{e}}}$ can also be computed in a similar way. The optimization for $\boldsymbol{\Theta}_{\mathrm{B}}$ is similar to that for $\boldsymbol{\Theta}_{\mathrm{A}}$ can be carried out in the same iteration.

The above procedure is repeated until the fractional increase of the objective value is below a threshold $\varepsilon_{\mathrm{GCE}}$. This scheme also inevitably increases the complexity. The complexity of the GCE algorithm mainly comes from steps 2, 5, and 6. In step 2, we need to compute $\left\{\xi_{\mathrm{A},m}\right\}_{m=1}^{M}$ and $\left\{\xi_{\mathrm{B},m}\right\}_{m=1}^{M}$. Therefore, the complexity of this part is $\mathcal{O}\left(M\left(N_{\mathrm{A}} + N_{\mathrm{B}}\right)\right)$. In step 5, we calculate elites' weights with the complexity $\mathcal{O}\left(M_{\mathrm{e}}\right)$. Finally, in step 6, the probability parameter $\mu_{\mathrm{A},l,n}^{(i+1)}$ and $\mu_{\mathrm{A},l,n}^{(i+1)}$ are updated with the complexity $\mathcal{O}\left(M_{\mathrm{e}}\left(N_{\mathrm{A}} + N_{\mathrm{B}}\right)\right)$. In summary, after I iterations, the total computational complexity of the proposed GCE -based scheme is $\mathcal{O}\left(IM\left(N_{\mathrm{A}} + N_{\mathrm{B}}\right)\right)$. Since I and M also do not have to be very large, we can conclude that the complexity of the proposed GCE-based scheme is acceptable.

C. OPTIMAL POWER ALLOCATION – OPA

For a two-hop system with a DF relay, the maximum spectral efficiency is achieved when both hops enjoy the same received SNR. Therefore, the power allocation optimization problem can be solved by $\mathbb{E}(\gamma_{\mathrm{R}}) = \mathbb{E}(\gamma_{\mathrm{D}})$. We assume that the total transmit power of S and R is fixed, i.e., $P = P_1 + P_2$ is a constant. We can get the optimal transmit power of the first hop by $P_2^{\mathrm{opt}} = P - P_1^{\mathrm{opt}}$ as

$$P_1^{\mathrm{opt}} = \frac{\mathrm{P}\gamma_2\left(\gamma_{\mathrm{ri}} + \sigma_n^2\right)}{\sigma_n^2\gamma_1 + \gamma_2\left(\gamma_{\mathrm{ri}} + \sigma_n^2\right)}. \quad (56)$$

$$\frac{1}{M_{\mathrm{e}}} \sum_{m=1}^{M_{\mathrm{e}}} \omega_{\mathrm{A},m}^{(i)} \left(\frac{\Omega\left(\varphi^{(i)}(\mathrm{A}, n), \mathcal{F}(l)\right)}{\mu_{\mathrm{A},l,n}^{(i)}} - \frac{1 - \Omega\left(\varphi^{(i)}(\mathrm{A}, n), \mathcal{F}(l)\right)}{1 - \mu_{\mathrm{A},l,n}^{(i)}} \right) \quad (54)$$

TABLE 1. Simulation and algorithmic parameters.

Parameters	Values	Parameters	Values
Location of S	(0m, 0m)	γ_{ri}	1 dBW
Location of A	(50m, 10m)	v	1/1.2
Location of R	(100m, 0m)	β_{s}	0.01
Location of B	(150m, 10m)	$P_{\mathrm{c}}^{\mathrm{S}}$	39 dBm
Location of D	(200m, 0m)	$P_{\mathrm{c}}^{\mathrm{D}}$	10 dBm
N_{S}	32	$P_{\mathrm{c}}^{\mathrm{R}}$	10 dBm
N_{R}	32	P_{c0}	20 dBm
N_{A}	32	$P_n(1)$	5 dBm
N_{B}	32	$P_n(2)$	15 dBm
f	28 GHz	$P_n(\infty)$	25 dBm
P	30 dBm	P_{A}	10 dBm

The ESE given in (7) for the proposed scheme with OPA is upper bounded by

$$\mathcal{R}_{\mathrm{up,OPA}} = \log_2\left(1 + \frac{P\gamma_1\gamma_2}{\sigma_n^2\gamma_1 + \left(\gamma_{\mathrm{ri}} + \sigma_n^2\right)\gamma_2}\right). \quad (57)$$

When both the OPS values and OPA are used simultaneously, the maximum ESE can be obtained as (58), shown at the bottom of the page.

V. SIMULATION RESULTS AND DISCUSSION

In this section, we present and discuss numerical results for the proposed system. All presented illustrations have been averaged results over 2000 independent channel realizations, whose parameters are summarized in Table 1. The noise power is given by $\sigma_n^2 = WN_0N_f = -94$ dBm, where W is the bandwidth, N_0 is the noise power spectral density, and N_f is the noise figure. We set the Rician-K factors $K_{\mathrm{SA}} = K_{\mathrm{BD}} = K_{\mathrm{AR}} = K_{\mathrm{RB}} = K = 10$ dB. In the Table 1, we also include the hardware dissipation parameters for source, RIS, and the destination, as well as for the DF relay that will be used for performance comparisons according to [25] and [27].

We first plot the ESE curves versus P under different models and test the tightness of the upper bounds in (23) and (32). As shown in Fig. 2, the results of upper bounds (with"upp") match well with the Monte Carlo simulation results (with "sim"). The results also demonstrate the superiority of the proposed hybrid FD DF relay and RISs system. With the increase of P, the performance gap between the FD relay-aided systems and the HD relay-aided system becomes larger. We set $\rho = 0.8$ in this simulation. Although the RISs provide good performance gain under OPS, the performance of the system equipped with "Only RISs" is worse than that of the proposed system because of the large path loss and the lack of LoS paths from A to B. Moreover, the system

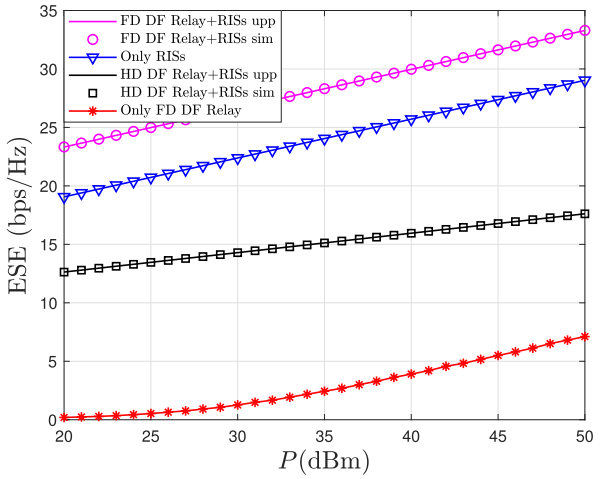

FIGURE 2. ESE versus P under different systems.

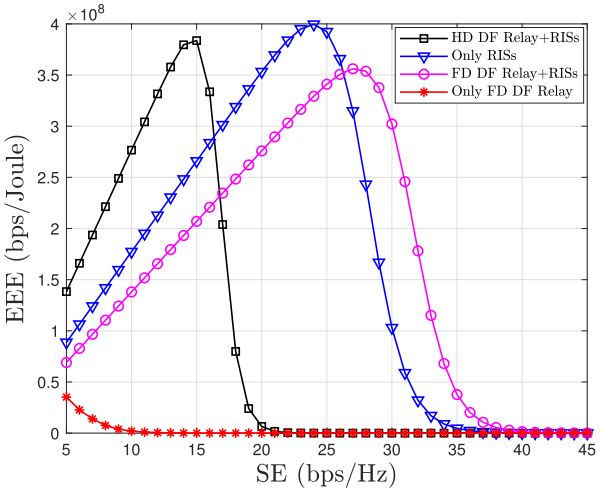

FIGURE 3. EEE versus required SE.

equipped with "Only RIS" would be worse than the proposed system with smaller ρ due to the impact of multi-hop RIS-aided reflections, showed in Fig. 9. For the system with "Only Relay", it is difficult to overcome large path loss and penetration loss because it can only obtain gain from a few traditional antennas.

Fig. 3 demonstrates the relationship between the EEE and the required SE for different system. First, we find out that the EEE of the three modes (except for the system equipped with "Only Relay") first increase to a maximum value, then decrease, and finally keep as constants over the required SE. We observe that the system equipped with "Only RISs" get the best performance when $16 < SE < 26$. This benefits from the passive nature of the RIS. The proposed "FD+RISs" and "HD+RISs" aided systems perform

$$\mathcal{R}_m = \log_2\left(1 + \frac{P\left(\mathcal{K}_1\rho^2N_{\mathrm{A}}^2N_{\mathrm{S}} + \mathcal{K}_2\rho^2N_{\mathrm{S}}N_{\mathrm{A}} + \tilde{\eta}_{\mathrm{SR}}N_{\mathrm{S}}\right)\left(\mathcal{K}_3\rho^2N_{\mathrm{B}}^2N_{\mathrm{R}} + \mathcal{K}_4\rho^2N_{\mathrm{R}}N_{\mathrm{B}} + \tilde{\eta}_{\mathrm{RD}}N_{\mathrm{R}}\right)}{\sigma_n^2\left(\mathcal{K}_1\rho^2N_{\mathrm{A}}^2N_{\mathrm{S}} + \mathcal{K}_2\rho^2N_{\mathrm{S}}N_{\mathrm{A}} + \tilde{\eta}_{\mathrm{SR}}N_{\mathrm{S}}\right) + \left(\gamma_{\mathrm{ri}} + \sigma_n^2\right)\left(\mathcal{K}_3\rho^2N_{\mathrm{B}}^2N_{\mathrm{R}} + \mathcal{K}_4\rho^2N_{\mathrm{R}}N_{\mathrm{B}} + \tilde{\eta}_{\mathrm{RD}}N_{\mathrm{R}}\right)}\right) \quad (58)$$

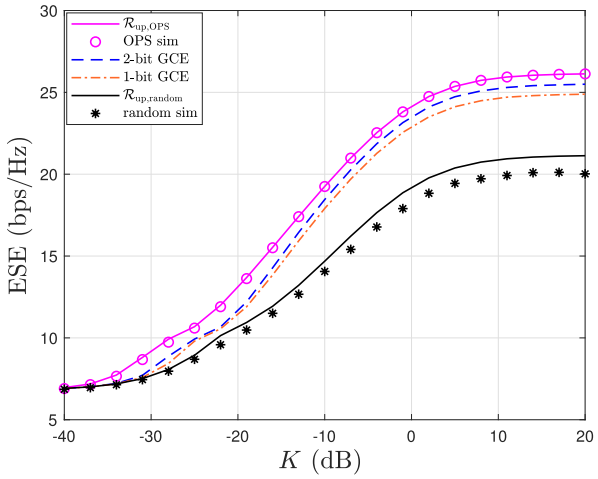

FIGURE 4. ESE versus K.

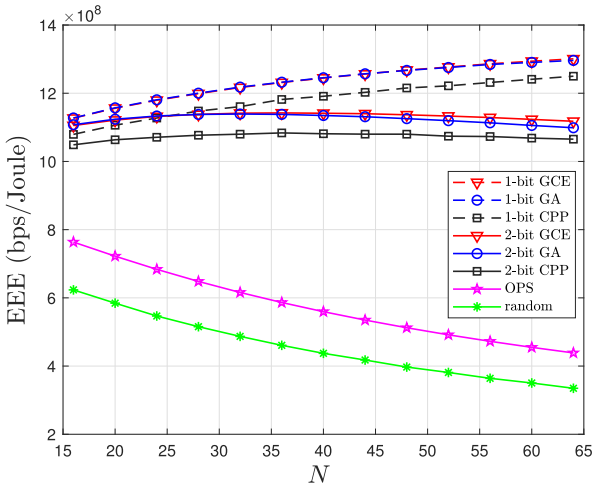

FIGURE 5. EEE versus N fixing $N_{\text{A}} = \frac{N}{2}$ and $N_{\text{B}} = \frac{N}{2}$.

good at high SE and low required SE, respectively. Despite the increased power consumption of the relay, our proposed system can improve performance while saving energy consumption.

Fig. 4 plots ESE curves versus the Rician K-factor. For the OPS-based design, the upper bound $\mathcal{R}_{\text{up,OPS}}$ is tightly close to the Monte-Carlo simulation results. When the Rician K-factor increases, the gap between the upper bound and the Monte-Carlo simulation diminishes. This demonstrates that the derived upper bound is applicable to both Rayleigh and Rician channels. Fig. 4 also demonstrates the correctness of the upper bounds $\mathcal{R}_{\text{up,OPS}}$ and $\mathcal{R}_{\text{up,random}}$ in (45) and (46), respectively. As discussed, these bounds are helpful in optimizing power allocation as well as to optimally arrange the positions of the RISs and the relay. When K is close to 0, the ESE becomes a constant and is not affected by the phase shifts design (as discussed in Case 1). When the Rician K-factor grows to infinity, the ESE approaches a stable value (as discussed in Case 2). The performance of the scheme based on random phase shifts is much poorer than performance of the schemes based on the proposed continuous and discrete phase shifts designs. For the GCE-base schemes, we set $M = 80$ and $\varepsilon_{\text{GCE}} = 10^{-4}$. Although the performance of the low resolution scheme (1-bit) is lower than that of the high resolution schemes (2-bit and OPS), it has the advantage of low power consumption, which will be analyzed in Fig. 5.

According to the close-form expressions of the upper bounds (23) and (45), we find that the ESE increases with increasing N_{A} and N_{B}. However, because the power consumption of RISs also increases due to the increase of the phase shifters, the relationship between EEE and the number of elements is uncertain. We assume that $N = N_{\text{A}} + N_{\text{B}}$. Fig. 5 plots the EEE curves for various schemes versus N with $N_{\text{A}} = N_{\text{B}} = \frac{N}{2}$. For the benchmark scheme based on Genetic Algorithm (GA) [32], we set the number of population individuals to $M = 80$ and the precision to $\varepsilon_{\text{GCE}} = 10^{-4}$ same as GCE. Although GA-based scheme have similar performance and complexity (equal to $\mathcal{O}(IM(N_{\text{A}} + N_{\text{B}}))$) to that of the proposed GCE-based scheme, the number of iterations I of GA (about 45 times) is much higher than that of the GCE (about 6 times). Moreover, the number I of GA increase with the number of elements and the performance of GA-based scheme is lower than that of the proposed GCE-based scheme in high N. The EEE of the "OPS" and "random" schemes decreases rapidly with increasing N. Although the "OPS" scheme shows the optimal performance in Fig. 4, its energy efficiency is lower than that of the schemes with discrete phase shifts (i.e., "GCE", "GA" and "CPP") due to the high power consumption caused by high bits. In contrast, for the schemes with discrete phase shifts, when quantified with 2 bits, the performance increases slightly and then decreases slightly with N. However, they are worse than that of the 1-bit quantification, in which the EEE continuously increases with N. Compared to the slight spectral efficiency loss, the high energy efficiency brought by the 1-bit quantization is attractive over high number of elements.

Fig. 6 plots the ESE curves for various schemes versus N_{A}, which satisfies $N_{\text{A}} \neq N_{\text{B}}$. Increasing N_{A} means decreasing N_{B} while keeping N unchanged. The OPA-based schemes are still always better than the equal power allocation (EPA)-based schemes. The performance of all schemes first increase as N increases, and then decrease when N exceeds the certain values. This phenomenon is related to the characteristic of the DF relay. Under the initial conditions of the simulation, the received SNR of the first hop is smaller than that of the second hop. The ESE of the first hop increases as N_{A} increases, until it equals the ESE of the second hop (which is decreasing). We can speculate that if the received SNR of the first hop under the initial conditions is smaller than that of the second hop, the overall performance of the system decreases as N_{A} increases. This observation also suggests that the total number of reflecting elements should be properly allocated between the two RISs in order to achieve the best overall performance.

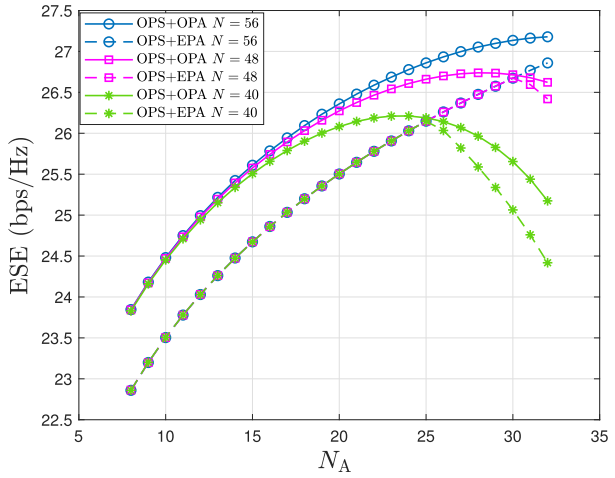

FIGURE 6. ESE versus N_{A} fixing N.

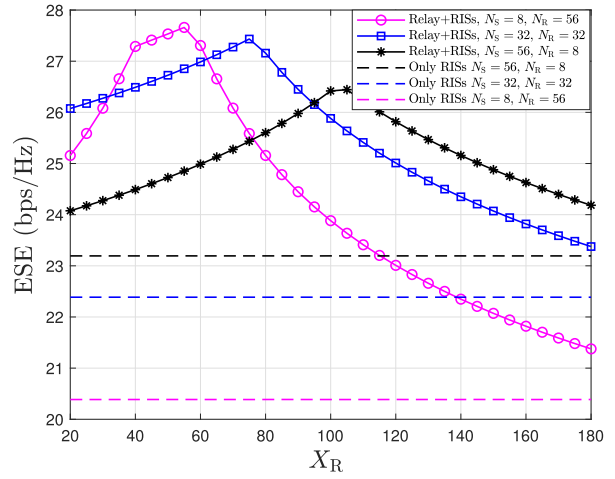

FIGURE 7. ESE versus X_{R}.

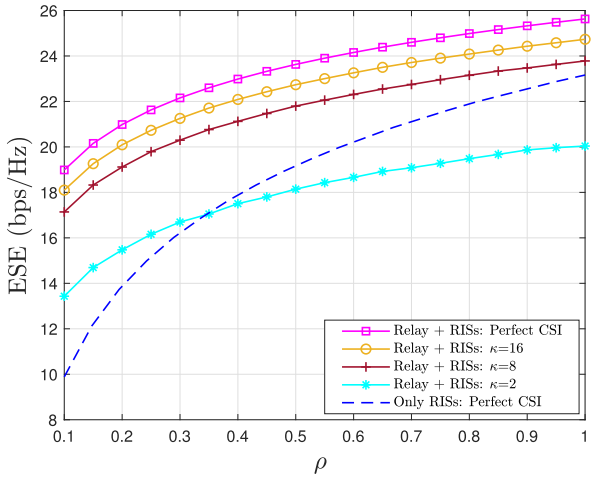

FIGURE 8. ESE versus the phase error and amplitude error.

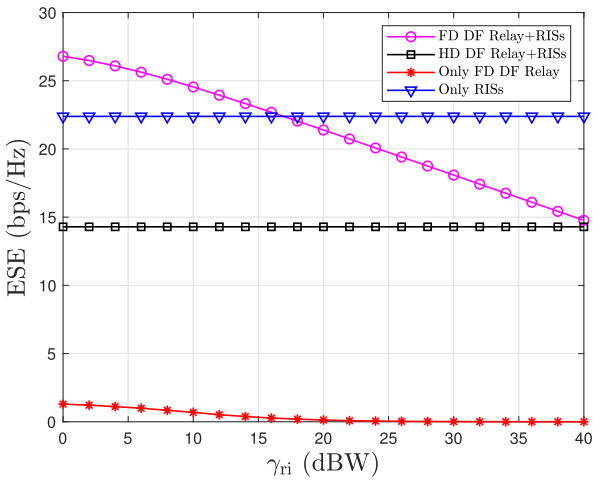

FIGURE 9. ESE versus γ_{ri}.

Fig. 7 demonstrates the EEE versus locations of the relay $(X_{\mathrm{R}}, 0)$. It demonstrates that the maximum of the ESE decreases as N_{R} decreases though the total number of active antennas keep unchanged. But the proposed hybrid FD DF relay and RISs system always outperforms the system aided only by RISs. Moreover, the optimal location of the relay will be closer to the destination as the number of antennas of the relay decreases. Accurate modeling is also important for determining the optimal position of the relay. For the case where the destination is indoor, we can place the relay near RIS B and the destination to eliminate the influence of large-scale fading, such as the penetration loss.

Because of the passive nature and the hardware impairments of RIS, the perfect channel status information (CSI) is usually unavailable and setting $\rho = 1$ is unjustified. We investigate the effect of the imperfect CSI and amplitude error on the system performance in Fig. 8. The error on each phase caused by imperfect CSI is modeled as a zero-mean von Mises variable whose concentration parameter κ captures the accuracy of the estimation [33]. The Fig. 8 indicates that performance gap between perfect CSI and $\kappa = 16$ is less than 1bps/Hz. But when $\kappa = 2$, the performance is 5 bps/Hz lower than that of perfect CSI, which is unacceptable. In addition, we can easily observe that the performance of the proposed system increases with increasing ρ. Compared with $\rho = 0.1$, the performance of $\rho = 1$ achieve 50% and 35% improvement in the $\kappa = 2$ and perfect CSI, respectively. Fig. 8 also demonstrates the performance of the system with only RISs suffers a lot when ρ is low. In particular, $\mathcal{R} = 9.88$ when $\rho = 0.1$ and $\mathcal{R} = 23.16$ when $\rho = 1$. It concludes that the SE is proportional to ρ^4. The SE of our proposed system is proportional to ρ^2 according to the upper bounds (23) and (45). Thus the system with only RISs is more sensitive to the amplitude error. Therefore, an efficient channel estimation scheme (high κ) and the reduction in hardware damage (high ρ) are crucial for the RIS to play its role in communication. Our proposed system can reduce the dependence on amplitude optimization of RIS, which is still a challenging problem to be addressed.

Fig. 9 highlights the importance of the self-interference cancellation accuracy to guarantee the advantages of such hybrid schemes. The proposed system outperforms the system with only RISs as long as the power of the residual self-interference is less than 16 dBW. In addition, the proposed hybrid system with a FD DF relay outperforms the hybrid system with a HD DF relay when γ_{ri} is less than 40 dBW. Finally, the proposed hybrid system is always better than that which only considers an FD DF relay to enhance link quality. This demonstrates that the performance of an DF FD relay can always be enhanced when combined with an RIS, as long as the phase-shifts are properly optimized.

VI. CONCLUSION

In this paper, a hybrid double-RIS and FD DF-relay aided system was proposed to assist an outdoor source to communicate with an indoor destination. Simulation results demonstrated the effectiveness of our proposed optimization schemes and the correctness of the upper bounds. The proposed OPS-based scheme obtain the best spectral efficiency, and the lower-cost GCE-based scheme shows advantages in both complexity and energy efficiency compared with the considered benchmarks. For the power allocation, the performance of the proposed OPA-based scheme is always better than that of the EPA-based scheme when the total power is fixed. Moreover, compared with the traditional systems, our proposed hybrid system can significantly improve the performance and effectively enhance communication between an outdoor source and an indoor destination.

REFERENCES

[1] Q. Wu and R. Zhang, "Towards smart and reconfigurable environment: Intelligent reflecting surface aided wireless network," *IEEE Commun. Mag.*, vol. 58, no. 1, pp. 106–112, Jan. 2020.

[2] E. Basar, M. Di Renzo, J. De Rosny, M. Debbah, M. Alouini, and R. Zhang, "Wireless communications through reconfigurable intelligent surfaces," *IEEE Access*, vol. 7, pp. 116753–116773, 2019.

[3] Q. Wu and R. Zhang, "Intelligent reflecting surface enhanced wireless network via joint active and passive beamforming," *IEEE Trans. Wireless Commun.*, vol. 18, no. 11, pp. 5394–5409, Nov. 2019.

[4] Q. Wu and R. Zhang, "Beamforming optimization for intelligent reflecting surface with discrete phase shifts," in *Proc. IEEE Int. Conf. Acoust., Speech Signal Process. (ICASSP)*, Brighton, U.K., May 2019, pp. 7830–7833.

[5] D.-W. Yue, H. H. Nguyen, and Y. Sun, "MmWave doubly-massive-MIMO communications enhanced with an intelligent reflecting surface: Asymptotic analysis," *IEEE Access*, vol. 8, pp. 183774–183786, 2020.

[6] P. Wang, J. Fang, X. Yuan, Z. Chen, and H. Li, "Intelligent reflecting surface-assisted millimeter wave communications: Joint active and passive precoding design," *IEEE Trans. Veh. Technol.*, vol. 69, no. 12, pp. 14960–14973, Oct. 2020.

[7] X. Li, J. Fang, F. Gao, and H. Li, "Joint active and passive beamforming for intelligent reflecting surface-assisted massive MIMO systems," 2019, *arXiv:1912.00728*.

[8] J. Lyu and R. Zhang, "Spatial throughput characterization for intelligent reflecting surface aided multiuser system," *IEEE Wireless Commun. Lett.*, vol. 9, no. 6, pp. 834–838, Jun. 2020.

[9] Y. Han, S. Zhang, L. Duan, and R. Zhang, "Cooperative double-IRS aided communication: Beamforming design and power scaling," *IEEE Wireless Commun. Lett.*, vol. 9, no. 8, pp. 1206–1210, Aug. 2020.

[10] C. Huang, Z. Yang, G. C. Alexandropoulos, K. Xiong, L. Wei, C. Yuen, Z. Zhang, and M. Debbah, "Multi-hop RIS-empowered Terahertz communications: A DRL-based hybrid beamforming design," *IEEE J. Sel. Areas Commun.*, vol. 39, no. 6, pp. 1663–1677, Jun. 2021.

[11] O. Özdogan, E. Björnson, and E. G. Larsson, "Intelligent reflecting surfaces: Physics, propagation, and pathloss modeling," *IEEE Wireless Commun. Lett.*, vol. 9, no. 5, pp. 581–585, May 2020.

[12] W. Tang, M. Z. Chen, X. Chen, J. Y. Dai, Y. Han, M. Di Renzo, Y. Zeng, S. Jin, Q. Cheng, and T. J. Cui, "Wireless communications with reconfigurable intelligent surface: Path loss modeling and experimental measurement," *IEEE Trans. Wireless Commun.*, vol. 20, no. 1, pp. 421–439, Jan. 2021.

[13] M. Di Renzo, K. Ntontin, J. Song, F. H. Danufane, X. Qian, F. Lazarakis, J. De Rosny, D. T. Phan-Huy, O. Simeone, R. Zhang, and M. Debbah, "Reconfigurable intelligent surfaces vs. relaying: Differences, similarities, and performance comparison," *IEEE Open J. Commun. Soc.*, vol. 1, pp. 798–807, 2020.

[14] E. Björnson, O. Özdogan, and E. G. Larsson, "Intelligent reflecting surface versus decode-and-forward: How large surfaces are needed to beat relaying?" *IEEE Wireless Commun. Lett.*, vol. 9, no. 2, pp. 244–248, Feb. 2020.

[15] X. Ying, U. Demirhan, and A. Alkhateeb, "Relay aided intelligent reconfigurable surfaces: Achieving the potential without so many antennas," 2020, *arXiv:2006.06644*.

[16] Z. Abdullah, G. Chen, S. Lambotharan, and J. A. Chambers, "A hybrid relay and intelligent reflecting surface network and its ergodic performance analysis," *IEEE Wireless Commun. Lett.*, vol. 9, no. 10, pp. 1653–1657, Oct. 2020.

[17] Z. Abdullah, G. Chen, S. Lambotharan, and J. A. Chambers, "Optimization of intelligent reflecting surface assisted full-duplex relay networks," *IEEE Wireless Commun. Lett.*, vol. 10, no. 2, pp. 363–367, Feb. 2021.

[18] I. Yildirim, F. Kilinc, E. Basar, and G. C. Alexandropoulos, "Hybrid RIS-empowered reflection and decode-and-forward relaying for coverage extension," *IEEE Commun. Lett.*, vol. 25, no. 5, pp. 1692–1696, May 2021.

[19] H. Q. Ngo, H. A. Suraweera, M. Matthaiou, and E. G. Larsson, "Multipair full-duplex relaying with massive arrays and linear processing," *IEEE J. Sel. Areas Commun.*, vol. 32, no. 9, pp. 1721–1737, Sep. 2014.

[20] T. Riihonen, S. Werner, and R. Wichman, "Hybrid full-duplex/half-duplex relaying with transmit power adaptation," *IEEE Trans. Wireless Commun.*, vol. 10, no. 9, pp. 3074–3085, Sep. 2011.

[21] G. Zheng, I. Krikidis, and B. Ottersten, "Full-duplex cooperative cognitive radio with transmit imperfections," *IEEE Trans. Wireless Commun.*, vol. 12, no. 5, pp. 2498–2511, May 2013.

[22] (2015). *5G Channel Model for Bands Up to 100 GHz*. [Online]. Available: http://www.5gworkshops.com/5GCM.html

[23] M. K. Samimi, S. Sun, and T. S. Rappaport, "MIMO channel modeling and capacity analysis for 5G millimeter-wave wireless systems," in *Proc. 10th Eur. Conf. Antennas Propag. (EuCAP)*, Apr. 2016, pp. 1–5.

[24] H. A. Suraweera, H. Q. Ngo, T. Q. Duong, C. Yuen, and E. G. Larsson, "Multi-pair amplify-and-forward relaying with very large antenna arrays," in *Proc. IEEE Int. Conf. Commun. (ICC)*, Budapest, Hungary, Jun. 2013, pp. 4635–4640.

[25] C. Huang, A. Zappone, G. C. Alexandropoulos, M. Debbah, and C. Yuen, "Reconfigurable intelligent surfaces for energy efficiency in wireless communication," *IEEE Trans. Wireless Commun.*, vol. 18, no. 8, pp. 4157–4170, Aug. 2019.

[26] Z. Gao, R. Qiu, C. Cai, J. Xue, C. Wang, and S. Chen, "Energy efficiency comparison for full-duplex DF and AF relaying protocols," in *Proc. 2nd Int. Conf. Comput. Commun. Internet (ICCCI)*, Jun. 2020, pp. 45–50.

[27] J. Ma, C. Huang, and Q. Li, "Energy efficiency of full- and half-duplex decode-and-forward relay channels," *IEEE Internet Things J.*, vol. 9, no. 12, pp. 9730–9748, Jan. 2022.

[28] L. You, J. Xiong, D. W. K. Ng, C. Yuen, W. Wang, and X. Gao, "Energy efficiency and spectral efficiency tradeoff in RIS-aided multiuser MIMO uplink transmission," *IEEE Trans. Signal Process.*, vol. 69, pp. 1407–1421, 2021.

[29] W. Zhang, J. Xu, W. Xu, D. W. K. Ng, and H. Sun, "Cascaded channel estimation for IRS-assisted mmWave multi-antenna with quantized beamforming," *IEEE Commun. Lett.*, vol. 25, no. 2, pp. 593–597, Feb. 2021.

[30] X. Gao, L. Dai, Y. Sun, S. Han, and I. Chih-Lin, "Machine learning inspired energy-efficient hybrid precoding for mmWave massive MIMO systems," in *Proc. IEEE Int. Conf. Commun. (ICC)*, May 2017, pp. 1–6.

[31] W. Chen, X. Ma, Z. Li, and N. Kuang, "Sum-rate maximization for intelligent reflecting surface based terahertz communication systems," in *Proc. IEEE/CIC Int. Conf. Commun. Workshops China (ICCC Workshops)*, Aug. 2019, pp. 153–157.

[32] K. Zhi, C. Pan, H. Ren, and K. Wang, "Statistical CSI-based design for reconfigurable intelligent surface-aided massive MIMO systems with direct links," *IEEE Wireless Commun. Lett.*, vol. 10, no. 5, pp. 1128–1132, May 2021.
[33] M. Badiu and J. P. Coon, "Communication through a large reflecting surface with phase errors," *IEEE Wireless Commun. Lett.*, vol. 9, no. 2, pp. 184–188, Feb. 2020.

GUANG-HUI LI received the B.S. degree in communication engineering from Henan Polytechnic University, Jiaozuo, China, in 2018. He is currently pursuing the Ph.D. degree in information and communication engineering with Dalian Maritime University, Dalian, China. His research interests include massive MIMO systems, millimeter wave communication, and intelligent reflecting surface.

DIAN-WU YUE (Senior Member, IEEE) received the B.S. and M.S. degrees in mathematics from Nankai University, Tianjin, China, in 1986 and 1989, respectively, and the Ph.D. degree in communications and information engineering from the Beijing University of Posts and Telecommunications, Beijing, China, in 1997. From 2000 to 2001, he was a Visiting Scholar at the University of Manitoba, Winnipeg, MB, Canada. From 2001 to 2002, he was a Postdoctoral Fellow at the University of Waterloo, Waterloo, ON, Canada. Since December 2003, he has been a Full Professor of communications and information engineering with Dalian Maritime University (DMU), Dalian, Liaoning, China. He is currently the Chairperson of the Academic Committee, College of Information Science and Technology, DMU. His research interests include massive MIMO systems, millimeter wave MIMO communications, wireless optical communications, and reconfigurable intelligent surfaces.

SI-NIAN JIN (Member, IEEE) received the B.S. degree in communication engineering from Shandong University, Weihai, China, in 2014, and the M.S. and Ph.D. degrees in communications and information engineering from Dalian Maritime University (DMU), Dalian, China, in 2017 and 2021, respectively. He is currently a Lecturer of communications and information engineering with DMU. His research interests include massive MIMO, cell-free massive MIMO, and intelligent reflecting surface.

QING HU (Member, IEEE) is currently a Professor of information science and technology with the College of Dalian Maritime University. His recent work mainly focuses on the marine intelligent communication and navigation technology, intelligent ship networking technology, and e-navigation strategy. He is a member of the International Maritime Organization (IMO), the International Association of AIDS to navigation (IALA), the International Radio Telecommunication Union (ITU) Working Group on the development of international standards for maritime communications, the Beidou Navigation Expert Group of the Ministry of transport of China, and the 8th Committee of the Communication and Navigation Sub Committee of the Chinese society of navigation.